ChemPubSoc Europe

DOI: 10.1002/chem.201602444

CHEMISTRY
A European Journal
Communication

Molecular Rectification

Electronic Modulation of the SOMO–HOMO Energy Gap in Iron(III) Complexes towards Unimolecular Current Rectification

Lanka D. Wickramasinghe,[a] Shivnath Mazumder,[a] Kenneth K. Kpogo,[a] Richard J. Staples,[b] H. Bernhard Schlegel,[a] and Cláudio N. Verani*[a]

Dedicated to Prof. Robert Metzger on the occasion of his 75th birthday

Abstract: Amphiphilic five-coordinate iron(III) complexes with $\{N_2O_2Cl\}$ and $\{N_2O_3\}$ coordination spheres are studied to elucidate the roles of electronic structure on the mechanisms for current rectification. The presence of an apical chlorido or phenolato ligand plays a crucial role, and the $[Fe^{III}\{N_2O_2Cl\}]$ species supports an asymmetric mechanism while its $[Fe^{III}\{N_2O_3\}]$ counterpart seems to allow for unimolecular mechanism. The effects of electron-donating and electron-withdrawing substituents in the ligand frameworks are also considered.

Current rectification entails a directional flow of electric current and is fundamental to the conversion of alternating into direct current that permits information management.[1] Although Aviram and Ratner[2] envisioned molecular rectification with well-defined donor and acceptor units over four decades ago, molecular rectifiers based on transition-metal coordination complexes are a more recent development.[3–7] Aiming to improve effective design, the understanding of complex rectifiers requires proper elucidation of metal/ligand electronic contributions on current rectification mechanisms. Our group has been at the forefront of complex rectifiers[8,9] and has evaluated the redox and electronic behavior of five-coordinate species $[Fe^{III}(L^1)Cl]$ (**1**) and $[Fe^{III}(L^3)]$ (**3**) with phenolate-rich tetradentate and pentadentate ligands (Scheme 1). These ligands bind strongly to an iron(III) cation to form low-symmetry, high-spin metallosurfactants that show excellent molecular rectification properties when Langmuir–Blodgett (LB) monolayers of these complexes are embedded between two gold electrodes in an Au|LB|Au device. Molecular rectification may happen though formation of Schottky barriers, asymmetric, or unimolecular electron transfer (ET).[1,10–12] The use of physisorbed LB films minimizes or eliminates the Schottky pathway.[13] In the asymmetric mechanism, the lowest unoccupied molecular orbital (LUMO) of the molecule is energetically closer to the Fermi levels of the Au electrodes and the highest occupied HOMO is much lower in energy, thus being unable to contribute to electron transfer. We have recently proposed[9] the involvement of singly occupied MOs, rather than unoccupied MOs, in complex rectifiers so that the Fermi/SOMO gap governs asymmetric rectification. In contrast, the unimolecular pathway primarily observed for organic systems[10–12,14–16] involves both the HOMO and LUMO (or SOMO in complexes) in ET as the HOMO of the donor is energetically comparable to the Fermi level of one electrode, while the LUMO/SOMO of the acceptor moiety is comparable to the second electrode. Therefore, we can anticipate that the closer the energy of the singly occupied SOMO of an Fe^{III} complex to the Fermi levels of the Au electrodes, the more favored is the asymmetric pathway. On the other hand, having both the SOMO and HOMO closer to the Fermi levels of the electrodes should lead to a unimolecular mechanism in which both SOMO and HOMO contribute to the rectification process.

Herein, we investigate the effects of electronic structure in modulating the SOMO–Fermi–HOMO energy gap in four high-spin iron(III) complexes (Scheme 1), thus aiming to demonstrate viability of unimolecular rectification and expanding the current definitions of molecular rectifiers.

We recently reported[9] that the relevant SOMO in the complex $[Fe^{III}(L^1)Cl]$ (**1**) is described as a linear combination of

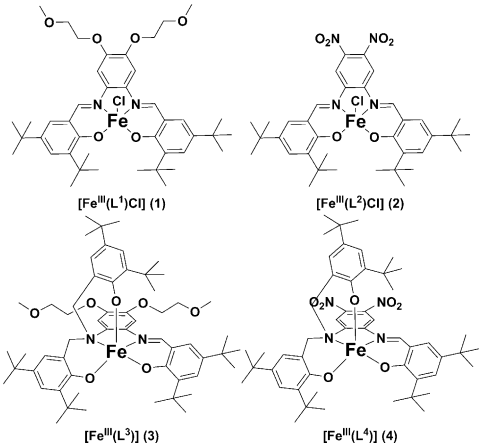

Scheme 1. The five-coordinate iron(III) complexes **1**–**4**.

[a] L. D. Wickramasinghe, Dr. S. Mazumder, K. K. Kpogo, Prof. H. B. Schlegel, Prof. C. N. Verani
Department of Chemistry, Wayne State University
5101 Cass Ave, Detroit, MI 48202 (USA)
E-mail: cnverani@chem.wayne.edu

[b] Dr. R. J. Staples
Department of Chemistry, Michigan State University
Lansing, MI 48824 (USA)

Supporting information for this article is available on the WWW under http://dx.doi.org/10.1002/chem.201602444.

$3d_{xz}+3d_{yz}$ molecular orbitals with predominant metal character. This is the lowest lying SOMO in a five-coordinate ^{HS}iron(III) ion with an idealized square pyramidal C_{4v} configuration $e(d_{xz}^1+d_{yz}^1)$ $b_2(d_{xy}^1)$ $a_1(d_{z^2}^1)$ $b_1(d_{x^2-y^2}^1)$. Asymmetric rectification is attributed to the 1 e^- reduction of this SOMO followed by rapid ET to the Au electrode without participation of the HOMO. The $3d_{xz}+3d_{yz}$ MOs are only 1 eV above the Fermi levels of the electrodes and are therefore energetically compatible.[9] The HOMO is centered on the phenylenediamine moiety and is 1.4 eV below the Fermi levels, and is thus too low in energy to take part in current rectification. Complex [$Fe^{III}(L^3)$] (**3**) with a tris(phenolate) ligand scaffold is expected to have a different elelctronic structure with a HOMO based on the phenolate moiety, rather than on the phenylenediamine. We hypothesize that changes in the nature (and hence the energy) of the HOMO, together with a change in the molecular geometry from distorted square pyramidal **1** to distorted trigonal bipyramidal **3** may alter the preferred mechanism of rectification. Moreover, replacement of the electron-donating alkoxo, $-O(CH_2)_2(OCH_3)$, substituent with the electron-withdrawing nitro, $-NO_2$, function in the ligand framework may further decrease the SOMO energy permitting lower applied potentials for molecular rectification. Similar electronic tune-ups have been proposed recently for other iron species.[17–19]

Complexes **1** and **3** were reported elsewhere.[8,9] The ligand H_2L^2 (Scheme 2) was obtained by treating two equivalents of 3,5-di-*tert*-butyl-2-hydroxybenzaldehyde with one equivalent of 4,5-dinitrobenzene-1,2-diamine[20] in methanol. The resulting mixture was refluxed for 28 h and the purified ligand was recrystallized from methanol. The ligand H_3L^4 was synthesized by reacting one equiv of 4,5-dinitrobenzene-1,2-diamine with four equiv of 2,4-di-*tert*-butyl-6-(chloromethyl) phenol. The ligand was purified by column chromatography.

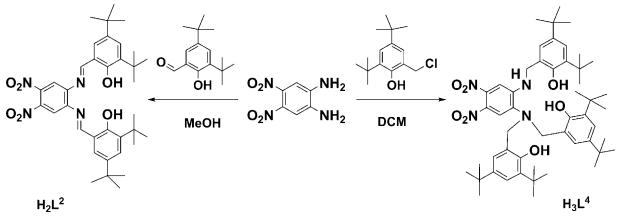

Scheme 2. Synthesis of ligands H_2L^2 and H_3L^4.

Complexes **2** and **4** were obtained by treating one equiv of the appropriate ligand with one equiv of an iron(III) salt in presence of anhydrous $NaOCH_3$. The FTIR spectroscopic data for **2** and **4** showed peaks at 1360 and 1470 cm^{-1} corresponding to the N=O stretching of the $-NO_2$ groups and peaks at 1573 cm^{-1} associated with C=N stretching vibrations. The high-resolution ESI-MS data showed molecular ion peaks [M^+] at $m/z=684.2610$ for **2** and [$M+H^+$] at $m/z=904.4453$ for **4**, in excellent agreement with the calculated masses. X-ray diffraction afforded unambiguous structure determination for both complexes as illustrated by their ORTEP plots (Figure 1; Supporting Information, Figure S1, Tables S1, S2). Complex **2**

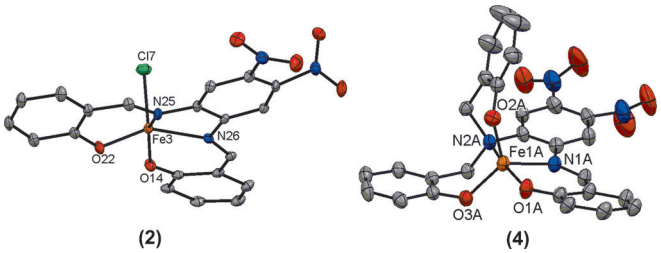

Figure 1. ORTEP representations for **2** and **4**. Ellipsoids set at 50% probability; H atoms and *tert*-butyl groups are omitted for clarity.[41]

adopts a distorted square-pyramidal geometry with a τ value[21] of 0.15, while a distorted trigonal bipyramidal structure is revealed for **4** with a τ value of 0.60.

To gain understanding on the electronic structure of the parent compounds prior to engaging in ET associated with rectification, UV/Vis spectra of **2** and **4** were recorded in dichloromethane and compared to **1** and **3** (Supporting Information, Figure S2 and Table S3).

These complexes display bands at 400–600 nm typically seen in imine five-coordinate ^{HS}iron(III) complexes, including a near-UV band at ca. 325 nm ($\varepsilon=21\,900$ L mol^{-1} cm^{-1}) assigned to an LMCT process from the phenolate p_π to the d_{σ^*} of iron(III), along with two shoulder peaks. The first at ca. 455 nm ($\varepsilon=9800$) is assigned to an intra-ligand ILCT process from the phenolate p_π to the p_{π^*} of the azomethine moiety,[8] and the second at about 550 nm ($\varepsilon=6100$) is attributed to an LMCT process from the phenolate p_π to the d_{π^*} of the iron(III) center. Species **2** and **4** also show a band at about 370 nm associated with the $\pi\rightarrow\pi^*$ CT of the nitro groups. These attributions are in agreement with the literature,[18,22–24] and with DFT calculations that confirm the ^{HS}iron(III) ($3d^5$, $S=5/2$) configuration as energetically favored in **4** by ca. 17 kcal mol^{-1} over the low-spin configuration ($S=3/2$).

The redox properties of **2** and **4** were measured in 1.0×10^{-3} mol L^{-1} dichloromethane solutions using $TBAPF_6$ as the electrolyte, and are used to assess SOMO/HOMO energy gaps as the first reduction reflects the incorporation of one electron to the lowest-lying SOMO and the first oxidation is associated to the removal of an electron from the highest HOMO. Cyclic voltammograms (CVs) are shown in Figure 2, whereas the measured redox potentials with $|I_{pa}/I_{pc}|$ current ratios and ΔE_p

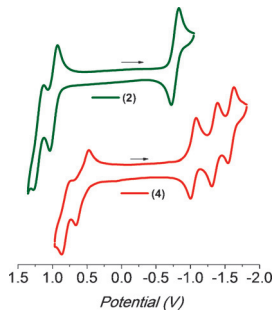

Figure 2. CVs of **2** and **4** in 1.0×10^{-3} mol L^{-1} dichloromethane solutions. Potentials plotted against the Fc^+/Fc couple.

values are reported in the Supporting Information, Table S4. The CV of **2** showed one reversible reduction event at -0.77 $V_{Fc+/Fc}$ attributed to the Fe^{III}/Fe^{II} redox couple. A few ill-defined cathodic events (see the Supporting Information, Figure S3 for details) were found between -1.0 and -2.5 $V_{Fc+/Fc}$ and are likely associated with the reduction of nitro groups. Two quasi-reversible oxidation processes observed at 0.99 and 1.2 $V_{Fc+/Fc}$ are ligand-centered, and delocalized over the coplanar phenolates.[25–27] Complex **4** shows the first reversible Fe^{III}/Fe^{II} reduction at -1.06 $V_{Fc+/Fc}$, therefore at a more negative potential due to the presence of a third apical phenolate. There are two additional reduction events at -1.36 and -1.61 $V_{Fc+/Fc}$. Complex **4** also displayed two quasi-reversible oxidative processes at 0.54 and 0.8 $V_{Fc+/Fc}$. In this case the anodic waves are attributed exclusively to phenolate/phenoxyl oxidation, in good agreement with the literature.[8,17,28–30]

DFT calculations[31] were performed on **4** to validate the redox and electronic assignments for these complexes. Indeed, Mulliken spin density (MSD) on iron decreases to 3.75 after the first reduction event suggesting the formation of a $^{HS}3d^6$ Fe^{II} ($S=4/2$, Figure 3A) and confirming the first reduction as being metal-based. The second reduction is *p*-nitro-based (Figure 3B) and can yield two nearly isoenergetic $S=3/2$ and 5/2 spin states, pending on the nature of the antiferromagnetic (AF) or ferromagnetic (F) coupling between the generated radical and the metal center.

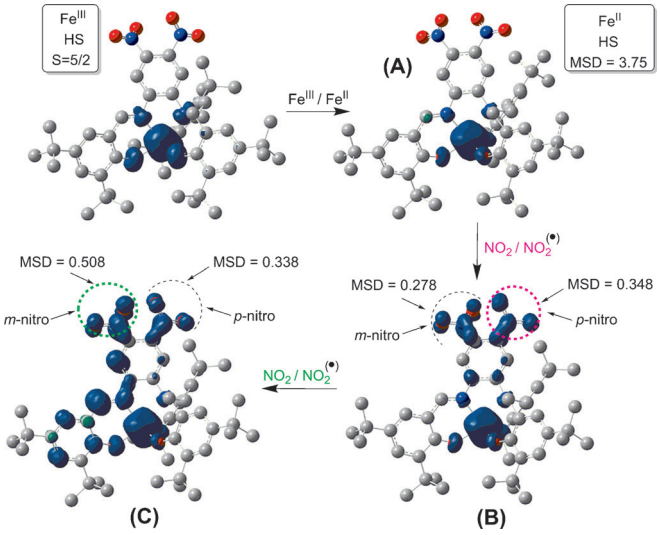

Figure 3. Spin density plots (isodensity 0.004 a.u.) and Mulliken spin density (MSD) values of the species involved in the CV profile of **4**.

The spin density plot for an F-coupled ($S=5/2$) configuration showed MSD values of 0.348 and 0.278 on the *p*-nitro and *m*-nitro moieties, respectively. The two nitro groups are nearly coplanar and electronically coupled, and the charge is delocalized over both nitro functionalities. The structure shown in Figure 3C was obtained after a third reduction event and showed considerable delocalization of spin density over the azomethine moiety and one phenolate ring. Inspection of the two nitro groups revealed that the spin density value of 0.338 on the *p*-nitro moiety in **C** is comparable to that in the doubly reduced species **B** at 0.348, while the spin density on the *m*-nitro group has significantly increased from 0.278 to 0.508. Thus, the third reduction is *m*-nitro-based. The calculated redox profile of **2** is shown in the Supporting Information, Figure S5, and is similar to **4** with a metal-based first reduction process.

Further evidence for the metal-centered nature of the first reduction comes from spectroelectrochemical analysis of **4** as performed at an applied potential of -1.1 $V_{Fc+/Fc}$ (Figure 4). Bands in the region of 550–800 nm decreased in intensity, while a new well-defined band appeared at 460 nm with an isosbestic point at 402 nm. Thus, upon reduction of iron(III) to iron(II) the phenolate-to-iron(III) LMCT disappears and is replaced by a new ILCT between the p_π phenolate oxygen and the p_{π^*} of the azomethine moiety.[9,32]

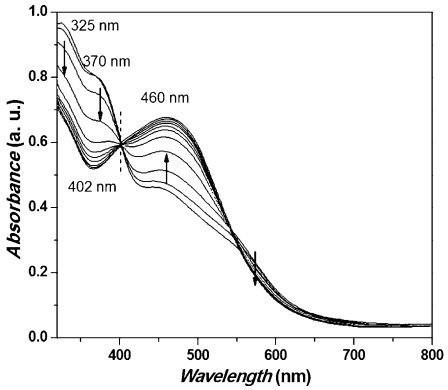

Figure 4. Electronic spectral changes observed during the first reduction for **4** under fixed potential conditions.

The electron transfer mechanisms contributing to the rectification properties have been evaluated by considering the changes in the nature and energy of the HOMOs from **1** to **3**. The electrochemical data and DFT calculations have shown that the metal centers behave as electron acceptors (A) and the ligand framework acts as electron donor (D). While Schottky mechanisms are less relevant due to the physisorbed nature of the LB monolayers, unimolecular or asymmetric mechanisms can be operative provided the respective molecular frontier orbitals display favorable energies.

To allow for ET by the amphiphilic complexes deposited as LB films between two electrodes, the Fermi levels (E_F) of the electrodes must be compatible with the energies of relevant molecular orbitals. For Au electrodes, $E_F \approx 5.1$ eV below vacuum,[33–35] and a proper matching between the E_F and HOMO/LUMO or HOMO/SOMO energies is a necessary requirement for an efficient electron transfer event between the two electrodes. The molecular redox potentials obtained from CV experiments can be transformed into solid-state potentials using the following equations: $V_a = 4.7\ eV + E_{1/2}{}^{red}{}_{SCE}$ and $V_i = 4.7\ eV + (1.7)\ E_{1/2}{}^{ox}{}_{SCE}$, where V_a and V_i are very close to the first electron affinity and first ionization energies of the amphiphile deposited on the electrodes, respectively,[36–39] and equivalent to the first metal-centered SOMO and first ligand-centered HOMO levels.

The $E_{1/2}{}^{red}{}_{SCE}$ and $E_{1/2}{}^{ox}{}_{SCE}$ are experimental half-wave first reduction and first oxidation potentials (vs. saturated calomel electrode) of the metal complex. Using measured redox potentials,[8,9] the SOMO levels are calculated as −4.1 and −3.6 eV for **1** and **3**, respectively, and the HOMO energies are −6.5 and −6.1 eV, respectively (Figure 5). This model shows that the SOMO of **3** lies 1.5 eV above the Au Fermi level, while the SOMO of **1** at 1.0 eV is closer to the Fermi level than that of **3**. The HOMO of **3** being at −6.1 eV is a close match to the Fermi level than that of **1**. These results indicate that the mechanisms of rectification are likely different for **1** and **3**. Complex **1** with an energetically favorable SOMO allows the electron transfer from one electrode to another without requiring involvement of the HOMO.[9] In contrast, **3** with its energetically accessible HOMO can support a [D-A] type structure. The transfer of an electron from the HOMO to the second Au electrode gives rise to the [D^+-A] state in **3**. Next, an excited electron populating the SOMO relaxes to occupy the semi-filled HOMO. This is followed by an electron transfer from the first Au electrode into the now empty SOMO to complete the electron transfer pathway between the Au|LB|Au device and through **3**. Complexes **2** and **4**, the electron-withdrawing nitro analogues of **1** and **3**, respectively, have also been studied with the hypothesis that the frontier molecular orbitals will become energetically more accessible in the former compounds facilitating the electron transfer and current rectification at even lower potentials than those[8,9] required for **1** and **3**.

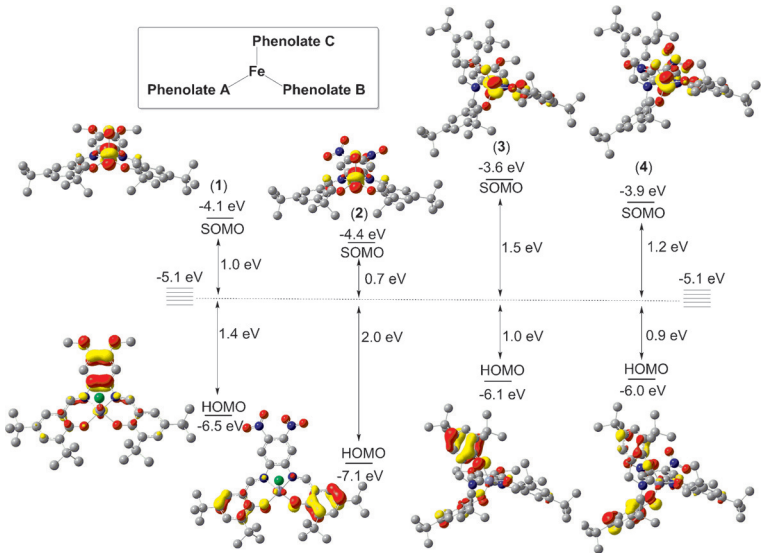

Figure 5. Comparison of HOMO, Fermi levels, and SOMO energies derived from experimental $E_{1/2}$ potentials and presented with calculated orbital models for $^{HS}Fe^{III}$ complexes **1**–**4**. Complexes **1** and **2** support an asymmetric pathway involving the metal-centered SOMOs, while **3** and **4** may favor a unimolecular mechanism inclusive of the ligand-centered HOMOs.

Indeed the SOMOs of **2** and **4** are lower than those for **1** and **3** by about 0.3 eV. Similarly, the HOMO of **2** is 0.6 eV lower when compared to that of **1**. Surprisingly, the HOMOs of **3** and **4** are nearly isoenergetic. These results are summarized in Figure 5 and allow us to propose that **1** and **2** with distorted square pyramidal $\{N_2O_2Cl\}$ coordination spheres will favor an asymmetric mechanism, while the distorted trigonal bipyramidal **3** and **4** with $\{N_2O_3\}$ coordination environments may allow for a unimolecular electron transfer pathway.

As illustrated in Figure 5, the SOMOs of complexes **1**–**4** can be described as a symmetry allowed linear combination of metal-centered $3d_{xz}+3d_{yz}$ orbitals, when the molecular *z*-axis is set either along the Fe–Cl for **1** and **2** or along the iron–apical phenolate (phenolate C) directions for **3** and **4**. The metal orbitals in **1** and **2** show an antibonding interaction with a p_π orbital of the apical chlorido ligand. This metal-apical ligand interaction increases in **3** and **4** as the Fe–O(phenolate C) bond distances are shorter by 0.39 Å compared to the Fe–Cl distances of **1** and **2**. The presence of a rigid $\{N_2O_3\}$ coordination sphere in **3** and **4** does not allow the Fe–O(phenolate C) bond to lengthen to minimize this antibonding interaction. As a result, the SOMOs of **3** and **4** increase in energy compared to those of **1** and **2**, and an asymmetric mechanism becomes less likely. Moreover, the nature of the ligand-centered HOMOs changes from phenylenediamine-centered in **1** to phenolate-based in **2**–**4**. The energy levels of the diminobenzene bridge and phenolate units are close and can be altered with proper substitution on the ligand frameworks.[40] The HOMO of square pyramidal **2** is delocalized over the two coplanar phenolate moieties. In contrast, the trigonal bipyramidal **3** and **4** have HOMOs centered on phenolate motifs A and C that are not coplanar.

Consequently, the HOMOs of **3** and **4** increase in energy and become closer to the Au Fermi levels than their respective SOMOs, thus fostering their involvement in a unimolecular mechanism. Unlike **1** and **2**, the energy levels of the HOMOs for **3** and **4** are not affected by the substitution of –ORO and $-NO_2$ on the ligand framework, since the HOMOs are nearly perpendicular to these groups with limited electronic communication.

Thus, considering 1) a proper match between the E_F and SOMO energy levels for **1** and **2**, and 2) the E_F and HOMO energies for **3** and **4**, an asymmetric mechanism can be proposed for the former complexes, whereas a unimolecular mechanism may be favored for the latter compounds.

In summary, we have successfully compared by means of experimental and theoretical approaches the behavior and associated MO energies of four iron(III) complexes with square pyramidal and trigonal bipyramidal geometries and with apical chloride or phenolate ligands. This careful comparison allowed us to postulate that the modulation of the SOMO–HOMO energy gaps can be attained to the presence of an appropriate apical ligand and/or substituent framework. On one hand if the energy of the SOMO can be approached to the E_F of the electrodes, asymmetric rectification will be favored and HOMO participation will be excluded. On the other hand, approaching the energy of the HOMO to the E_F of the electrodes may favor rectification towards a unimolecular pathway. The use of elec-

tronic modulation of orbitals to match the energy of Fermi levels in the electrodes expands the very concept of a molecular rectifier and allows for a rational design of future systems, thus moving rectification further afield. Efforts to incorporate complexes **2** and **4** into Au|LB|Au devices in order to measure their *I/V* curves are currently underway.

Acknowledgements

The experimental portion of this work was funded by the National Science Foundation through the grants NSF-CHE1012413 and CHE1500201 to C.N.V., and include financial support for L.D.W. and K.K.; The DFT calculations were funded by the U.S. Department of Energy, Office of Science, Basic Energy Sciences under the grant DE-SC0001907 to C.N.V. and H.B.S. and National Science Foundation through the grant CHE 1464450 to H.B.S., including financial support to S.M. Computer time allocated at the WSU–Grid System for the DFT is also acknowledged. L.D.W. and S.M. contributed equally to this study.

Keywords: coordination complexes · current rectification mechanisms · electron transfer · iron · molecular rectification

[1] R. M. Metzger, *Chem. Rev.* **2015**, *115*, 5056 – 5115.
[2] A. Aviram, M. Ratner, *Chem. Phys. Lett.* **1974**, *29*, 277 – 283.
[3] Y. Lee, S. Yuan, A. Sanchez, L. Yu, *Chem. Commun.* **2008**, 247 – 249.
[4] G. J. Ashwell, B. Urasinska, W. D. Tyrrell, *Phys. Chem. Chem. Phys.* **2006**, *8*, 3314 – 3319.
[5] M. H. Yoon, A. Facchetti, T. J. Marks, *Proc. Natl. Acad. Sci. USA* **2005**, *102*, 4678 – 4682.
[6] S. Roth, S. Blumentritt, M. Burghard, C. M. Fischer, G. Philipp, C.-M. Schwanneke, *Synth. Met.* **1997**, *86*, 2415 – 2418.
[7] W. J. Pietro, *Adv. Mater.* **1994**, *6*, 239 – 242.
[8] L. D. Wickramasinghe, M. M. Perera, L. Li, G. Mao, Z. Zhou, C. N. Verani, *Angew. Chem. Int. Ed.* **2013**, *52*, 13346 – 13350; *Angew. Chem.* **2013**, *125*, 13588 – 13592.
[9] L. D. Wickramasinghe, S. Mazumder, S. Gonawala, M. M. Perera, H. Baydoun, B. Thapa, L. Li, L. Xie, G. Mao, Z. Zhou, H. B. Schlegel, C. N. Verani, *Angew. Chem. Int. Ed.* **2014**, *53*, 14462 – 14467; *Angew. Chem.* **2014**, *126*, 14690 – 14695.
[10] R. M. Metzger, *J. Mater. Chem.* **2008**, *18*, 4364 – 4396.
[11] R. M. Metzger, *Chem. Rec.* **2004**, *4*, 291 – 304.
[12] R. M. Metzger, *Chem. Rev.* **2003**, *103*, 3803 – 3834.
[13] K. Ariga, Y. Yamauchi, T. Mori, J. P. Hill, *Adv. Mater.* **2013**, *25*, 6477 – 6512.
[14] W. J. Shumate, D. L. Mattern, A. Jaiswal, D. A. Dixon, T. R. White, J. Burgess, A. Honciuc, R. M. Metzger, *J. Phys. Chem. B* **2006**, *110*, 11146 – 11159.
[15] C. Krzeminski, C. Delerue, G. Allan, D. Vuillaume, R. M. Metzger, *Phys. Rev. B* **2001**, *64*, 085405-1-085405 – 6.
[16] R. M. Metzger, *Acc. Chem. Res.* **1999**, *32*, 950 – 957.
[17] C. Imbert, H. P. Hratchian, M. Lanznaster, M. J. Heeg, L. Hryhorczuk, B. R. McGarvey, H. B. Schlegel, C. N. Verani, *Inorg. Chem.* **2005**, *44*, 7414 – 7422.
[18] M. S. Shongwe, C. H. Kaschula, M. S. Adsetts, E. W. Ainscough, A. M. Brodie, M. J. Morris, *Inorg. Chem.* **2005**, *44*, 3070 – 3079.
[19] D. N. Bowman, A. Bondarev, S. Mukherjee, E. Jakubikova, *Inorg. Chem.* **2015**, *54*, 8786 – 8793.
[20] a) O. Siri, P. Braunstein, *New J. Chem.* **2005**, *29*, 75 – 79; b) A. Kleineweischede, J. Matty, *Eur. J. Org. Chem.* **2006**, 947 – 957; c) G. W. H. Cheeseman, *J. Chem. Soc.* **1962**, 1170 – 1176.
[21] A. W. Addison, T. N. Rao, J. Reedijk, J. van Rijn, G. C. Verschoor, *J. Chem. Soc. Dalton Trans.* **1984**, 1349 – 1356.
[22] U. Auerbach, U. Eckert, K. Wieghardt, B. Nuber, J. Weiss, *Inorg. Chem.* **1990**, *29*, 938 – 944.
[23] B. P. Gaber, V. Miskowski, T. G. Spiro, *J. Am. Chem. Soc.* **1974**, *96*, 6868 – 6873.
[24] K. K. Bania, D. Bharali, B. Viswanathan, R. C. Deka, *Inorg. Chem.* **2012**, *51*, 1657 – 1674.
[25] M. Orio, O. Jarjayes, H. Kanso, C. Philouze, F. Neese, F. Thomas, *Angew. Chem. Int. Ed.* **2010**, *49*, 4989 – 4992; *Angew. Chem.* **2010**, *122*, 5109 – 5112.
[26] T. Storr, P. Verma, Y. Shimazaki, E. C. Wasinger, T. D. P. Stack, *Chem. Eur. J.* **2010**, *16*, 8980 – 8983.
[27] R. C. Pratt, L. M. Mirica, T. D. P. Stack, *Inorg. Chem.* **2004**, *43*, 8030 – 8039.
[28] M. Lanznaster, H. P. Hratchian, M. J. Heeg, L. M. Hryhorczuk, B. R. McGarvey, H. B. Schlegel, C. N. Verani, *Inorg. Chem.* **2006**, *45*, 955 – 957.
[29] M. Lanznaster, M. J. Heeg, G. T. Yee, B. R. McGarvey, C. N. Verani, *Inorg. Chem.* **2007**, *46*, 72 – 78.
[30] M. M. Allard, J. A. Sonk, M. J. Heeg, B. R. McGarvey, H. B. Schlegel, C. N. Verani, *Angew. Chem. Int. ed.* **2012**, *51*, 3178 – 3182; *Angew. Chem.* **2012**, *124*, 3232 – 3236.
[31] R. G. Parr, W. Yang, *Density-functional theory of atoms and molecules*, Oxford University Press, New York, **1989**.
[32] D. Basu, M. M. Allard, F. R. Xavier, M. J. Heeg, H. B. Schlegel, C. N. Verani, *Dalton Trans.* **2015**, *44*, 3454 – 3466.
[33] L. Zhang, J. A. Bain, J. G. Zhu, L. Abelmann, T. Onoue, *IEEE Trans. Magn.* **2004**, *40*, 2549 – 2551.
[34] K. Kitagawa, T. Morita, S. Kimura, *Langmuir* **2005**, *21*, 10624 – 10631.
[35] K. Seo, A. V. Konchenko, J. Lee, G. S. Bang, H. Lee, *J. Am. Chem. Soc.* **2008**, *130*, 2553 – 2559.
[36] J. He, Q. Fu, S. Lindsay, J. W. Ciszek, J. M. Tour, *J. Am. Chem. Soc.* **2006**, *128*, 14828 – 14835.
[37] Scanning Tunneling Spectroscopy": K. W. Hipps in *Handbook of Applied Solid State Spectroscopy* (Ed.: D. R. Vij), Springer, Berlin, **2006**, chap. 7.
[38] L. Scudiero, D. E. Barlow, K. W. Hipps, *J. Phys. Chem. B* **2002**, *106*, 996 – 1003.
[39] A. Schmidt, N. R. Armstrong, C. Goeltner, K. Muellen, *J. Phys. Chem.* **1994**, *98*, 11780 – 11785.
[40] A. Kochem, O. Jarjayes, B. Baptiste, C. Philouze, H. Vezin, K. Tsukidate, F. Tani, M. Orio, Y. Shimazaki, F. Thomas, *Chem. Eur. J.* **2012**, *18*, 1068 – 1072.
[41] CCDC 1449044 (**2**) and 1449043 (**4**) contain the supplementary crystallographic data for this paper. These data are provided free of charge by The Cambridge Crystallographic Data Centre.

Received: May 23, 2016
Published online on June 27, 2016

